J Therm Anal Calorim (2014) 117:447–461
DOI 10.1007/s10973-014-3672-z

Comparison and validation of methods for estimating heat generation rate of large-format lithium-ion batteries

Jianbo Zhang · Jun Huang · Zhe Li · Bin Wu · Zhihua Nie · Ying Sun · Fuqiang An · Ningning Wu

Received: 14 October 2013 / Accepted: 27 January 2014 / Published online: 16 February 2014

Abstract The heat generation rate of a large-format 25 Ah lithium-ion battery is studied through estimating each term of the Bernardi model. The term for the reversible heat is estimated from the entropy coefficient and compared with the result from the calorimetric method. The term for the irreversible heat is estimated from the intermittent current method, the *V*–*I* characteristics method and a newly developed energy method. Using the obtained heat generation rates, the average cell temperature rise under 1C charge/discharge is calculated and validated against the results measured in an accelerating rate calorimeter (ARC). It is found that the intermittent current method with an appropriate interval and the *V*–*I* characteristics method using a pouch cell yield close agreement, while the energy method is less accurate. A number of techniques are found to be effective in circumventing the difficulties encountered in estimating the heat generation rate for large-format lithium-ion batteries. A pouch cell, using the same electrode as the 25 Ah cell but with much reduced capacity (288 mAh), is employed to avoid the significant temperature rise in the *V*–*I* characteristics method. The first-order inertial system is utilized to correct the delay in the surface temperature rise relative to the internal heat generation. Twelve thermocouples are used to account for the temperature distribution.

Keywords Lithium-ion battery · Heat generation rate · Energy method · *V*–*I* characteristics method · Intermittent current method

J. Zhang · J. Huang · Z. Li (✉) · B. Wu
Department of Automotive Engineering, State Key Laboratory of Automotive Safety and Energy, Tsinghua University, Beijing 100084, China
e-mail: lizhe1212@gmail.com

J. Huang
e-mail: huangjun12@mails.tsinghua.edu.cn

Z. Nie · Y. Sun · F. An · N. Wu
CITIC Guo'an MGL Power Technology Co., Ltd, Beijing 102200, China

Introduction

The lithium-ion battery is becoming the mainstream power sources for electric vehicles because of its high energy density and long cycle life [1]. However, the thermal issues, such as the potential risk of thermal runaway [2–4] and the stringent restriction on both the limits and the variation of the cell operation temperatures, constitute one of the bottlenecks for the widespread use of large-format lithium-ion batteries in electric vehicles. In addition to experimental investigation [1, 5, 6], thermal simulation is a powerful tool to elucidate the mechanism underlying these thermal issues [7, 8]. The fundamental governing equation used in the thermal simulation is the heat transfer equation:

$$\rho C_{\mathrm{P}} \frac{\partial T}{\partial t} = \nabla \cdot (k \nabla T) + q \tag{1}$$

where ρ is density, C_{p} is heat capacity, T is temperature, k denotes thermal conductivity, q is the heat generation rate per unit volume.

It is evident that the accuracy of the thermal simulation depends on the accuracy of the models to predict the heat generation rates for cells at different states and under various operation conditions. These heat generation rate models can be classified into two types. The first type is based on the thermal-electrochemical battery model and

provides deep insights into the underlying causes and detailed components of the heat generation [9, 10]. However, a large set of parameters, which describe the transport processes and electrochemical processes, are difficult to be determined. Therefore, the accuracy of the heat generation rate depends heavily on the parameters tuning procedure. The heat generation model of the second type is the simplified Bernardi heat generation model [11]:

$$Q = Q_{\text{rev}} + Q_{\text{irrev}} \tag{2}$$

$$Q_{\text{rev}} = IT\left(\frac{\partial U}{\partial T}\right)_{\text{P}} \tag{3}$$

$$Q_{\text{irrev}} = I(V - U) \tag{4}$$

where Q is the total heat generation rate of lithium-ion batteries, Q_{rev} is the reversible heat corresponding to the entropy change of the lithium intercalation/deintercalation reaction, Q_{irrev} is the irreversible heat generated from electrode polarization, V is the terminal voltage, U is the equilibrium potential, and I is the charge/discharge current, assumed to be positive during charge.

Bernardi model is solidly founded on physics and has much less parameters. It is the most widely used model in the thermal simulation of the battery. In practice, the irreversible heat generation rate is usually further simplified through defining an overpotential resistance, R, as:

$$R = (V - U)/I. \tag{5}$$

The irreversible heat generation rate equation now becomes:

$$Q_{\text{irrev}} = I^2R \tag{6}$$

Based on Eqs. (2–6), various methods have been developed [12–20] to estimate the reversible/irreversible heat generation for *small lithium-ion batteries* used in electronic devices. Much fewer works, however, have been found to study and to validate the heat generation rate for *large-format lithium-ion batteries*.

Regarding the reversible heat term, two methods, the potentiometric method and the calorimetric method, have been proposed and utilized [12–20]. The potentiometric method measured the equilibrium potential of the cell adjusted at certain SOC at various temperatures. Taking the derivative of the equilibrium potential with respect to the temperature gave the entropy coefficient, $\mathrm{d}U/\mathrm{d}T$. The calorimetric method measured the heat flows during charge and discharge. Assuming that the irreversible heat generation rates during charge and discharge were identical, the entropy coefficient was calculated from the difference of the heat flows. In [15, 16], the authors studied the entropy changes associated with the structural and phase changes in negative and positive electrodes. Using half-cell, they further quantified the individual contribution of each electrode [19]. Thomas et al. [20] concluded that, with proper correction for self-discharge, the potentiometric method was more accurate than the calorimetric method in calculating the reversible heat.

Regarding the irreversible heat term, Onda et al. [12–14] developed four methods: (1) the *V–I* characteristics method using voltage–current curves of discharge at a series of constant currents; (2) the OCV-V method using the difference between the open-circuit voltage and the terminal voltage; (3) the intermittent current method using the voltage change after 60 s of discharge at a constant current; (4) the AC impedance method.

Analysis of the previous literatures leads to the following observations:

Firstly, all the methods were originally developed for the small lithium-ion battery. Applying these methods to the large-format lithium-ion batteries will encounter a number of difficulties. One problem is the significant rise of temperature and the evolution of temperature variation across the cell even at moderate rates of charge/discharge [6]. Rising and non-uniform temperature makes it difficult to define a representative temperature for the measured overpotential resistance, which is strongly dependent on the battery temperature. Another problem is that there exists a considerable delay in the response of the surface temperature relative to the internal heat generation [6]. As a result, it is unconvincing to directly use the surface temperature at one point to calculate the heat generation rate and then to use it to validate the estimated values based on the Bernardi model.

Secondly, comparing the various methods can guide the selection of appropriate method to estimate the heat generation rate. Onda et al. [12–14] developed four methods to estimate the irreversible heat term, but they only compared these methods in terms of the overpotential resistance obtained using each method, and then without convincing reasons, they applied the *V–I* characteristics method alone to simulate the cell temperature rise. In addition, in [17, 18], only the intermittent current method was employed. Onda et al. [12–14] pointed out that the AC method gives much lower overpotential resistance than other three methods, hence it is not considered in this study. Besides, the OCV-V method is essentially the same as the *V–I* characteristics method when considering the OCV curve as the discharge curve at sufficiently small current, thus, only the *V–I* characteristics method is included here. The *V–I* characteristic method has problems in considerable temperature rise, while the intermittent current method relies on the selection of the calculation interval, which is somewhat arbitrary in the previous studies. Therefore, the implementation details of these methods need to be closely examined, and the accuracy needs to be compared and validated against measured results. In addition, a new

method, developed in our group and named energy method in this study, will also be included in the comparison.

Therefore, the objectives of this paper are to explore techniques to circumvent the above mentioned difficulties so as to extend, compare, and validate the various methods developed for small lithium-ion batteries to estimate the heat generation rate for large-format lithium-ion batteries. A large-format 25 Ah lithium-ion battery was used and its heat generation rate was studied based on the simplified Bernardi heat generation model. The potentiometric method and the calorimetric method were used to estimate the reversible heat. The intermittent current method, the *V–I* characteristics method and a newly proposed energy method were used to estimate the irreversible heat. The estimated values were compared and validated against the results measured in an ARC. A number of techniques, including the use of a pouch cell, the compensation of the time delay, and the use of 12 thermocouples to get the average cell temperature, were proposed to circumvent the problems encountered in dealing with large-format cells. The structure of this paper is as follows: "Method development" section introduces the methods employed in this study; "Experimental" section describes the experimental details; in "Results and discussion" section, firstly, we report the results of the entropy coefficient and overpotential resistance, secondly, we validate the estimated heat generation rate using the measured date by the ARC, finally, discussion concerning various methods is provided; "Conclusions" section is the conclusion.

Method development

The reversible heat

The potentiometric method

The term of the reversible heat generation rate was calculated by measuring the entropy coefficient $\mathrm{d}U/\mathrm{d}T$ as shown in Eq. (3). The equilibrium potential of the 25 Ah cell at a specified initial SOC was measured at a series of temperatures, and the entropy coefficient at this SOC was attained by calculating the slope of the fitted 'temperature-potential' line. Then the SOC of the cell was adjusted with a step length of 0.1 each time, and the entropy coefficient at each different SOC was obtained.

The calorimetric method

The calorimetric method assumed that the irreversible heat generation rates during charge and discharge were assumed to be identical under the same current amplitude I, and then the entropy coefficient was calculated by Eq. (7) based on Eq. (2):

$$\left(\frac{\partial U}{\partial T}\right)_{\mathrm{P}} = \frac{Q_{\mathrm{cha}} - Q_{\mathrm{dis}}}{2IT} \tag{7}$$

here, Q_{cha} and Q_{dis} are the total heat generation rate during charge and discharge, respectively, which were measured with the ARC or other calorimetric methods.

The irreversible heat

The V–I characteristics method

A series of constant-current charge or discharge tests at different C-rates are needed to explore the *V–I* characteristics of the battery [13]. Under a specified SOC and temperature, an approximate linear relationship between the terminal voltage and the applied current was found in the constant-current charge or discharge tests. As a result, the slope of the linearly fitted line gave the overpotential resistance, R_{VI}, of the *V–I* characteristics method [13].

The intermittent current method

The battery overpotential resistance is widely estimated from the intermittent charge or discharge at a definite SOC and temperature. The most frequently used intermittent current method to obtain the battery DC resistance is introduced in the HPPC test procedures [21]. The overpotential resistance, R_{IC}, was estimated by Eq. (8):

$$R_{\mathrm{IC}} = (V_{\mathrm{t}} - V_0)/I \tag{8}$$

where $(V_{\mathrm{t}} - V_0)$ is the voltage change after charging/discharging at current I (positive during charge) for time t, which is termed as the interval throughout this paper.

Different values of t have been used in the literature. For example, 4 h was adopted by Yang et al. [18], 30 s was adopted by Lu et al. [17], and 60 s was used in [12–14]. In the experimental part of this paper, a series of t (10, 30, 60, 90, 110 s) was applied and its effect on the accuracy of the estimation results was examined.

The energy method

The irreversible heat was calculated from the overpotential resistance in most of the previous studies [12–19]. In addition to these methods, a new method, which was inspired by the concept proposed in the work of Lv et al. [22], was developed in this study to calculate the irreversible heat directly. The new method is to be referred to as energy method hereafter.

(1) *Energy balance during charge* when charging the battery from SOC_1 to SOC_2, the total consumed energy from the power supply such as a

comprehensive tester or a charger, E_{cha}, consisted of three parts, the energy stored in the battery, E_{bat}, the energy corresponding to entropy change, $E_{rev,cha}$, and the energy dissipation by polarization, $E_{irrev,cha}$, as expressed in Eq. (9):

$$E_{cha} = E_{bat} + E_{rev,cha} + E_{irrev,cha}. \quad (9)$$

(2) *Energy balance during discharge* Similarly, when discharging the battery from SOC_2 back to SOC_1, the energy consumption, E_{bat}, also consisted of three parts, the electrical work performed by the battery, E_{dis}, the energy corresponding to entropy change, $E_{rev,dis}$, and the energy dissipation by polarization, $E_{irrev,dis}$, as shown in Eq. (10):

$$E_{bat} = E_{dis} + E_{rev,dis} + E_{irrev,dis}. \quad (10)$$

Since the E_{bat} terms in Eqs. (9) and (10) were identical, the irreversible heat could be calculated according to Eq. (11), which was the result of adding Eqs. (9) and (10) using the following two assumptions: first, the sum of the heat due to entropy change during charge and discharge process equaled zero, that is, $E_{rev,dis} + E_{rev,cha} = 0$. Second, the irreversible heat generation during charge and discharge at any temperature and SOC were identical, that is,

$$E_{irrev,dis} = E_{irrev,cha} = E_{iirev}.$$
$$E_{irrev} = (E_{cha} - E_{dis})/2 \quad (11)$$

According to the energy method, an overpotential resistance, R_{EM}, was defined as in Eq. (12) to facilitate the comparison with other methods which estimate the irreversible heat through the overpotential resistance:

$$R_{EM} = \frac{E_{cha} - E_{dis}}{2I^2 \Delta t}, \quad (12)$$

where I is the current and Δt is the duration of charge or discharge.

Direct measurement of the heat generation rate by the ARC

The ARC was used to provide an adiabatic environment for the cell placed in its chamber under the temperature feedback-and-chasing mode. When the cell underwent a charge or discharge process, its heat generation rate was calculated as in Eq. (13):

$$Q = mC_P \frac{dT}{dt}, \quad (13)$$

where m is the cell mass, C_p is the thermal capacity, dT/dt is the temperature rising rate, which was measured by the attached feedback thermocouples on the surface of the cell. The positions of the feedback thermocouples were strategically chosen to reflect the average temperature of the surface.

Experimental

A 25 Ah cell and a pouch cell were used in this study, which had the same cathode composited of $LiMn_xCo_yNi_zO_2$ and $LiMn_2O_4$, and the same graphite anode; the only differences were the size and capacity. The specifications of the two cells are shown in Table 1. Each fresh cell was cycled for five times before it was used in the heat measurement tests to ensure it had entered a stage of stable performance. During each cycle, the cell was first charged in a constant current-constant voltage (CC–CV) pattern with 1/3 C as the constant current charging rate, and then discharged at the same rate.

Four tests were conducted in this study to explore all the methods introduced in "Method development" section: (1) Test 1: the measurement of the entropy coefficient to estimate the reversible heat; (2) Test 2: the intermittent charge/discharge tests of the 25 Ah cell, which were used to calculate the overpotential resistance both by the intermittent current method and the energy method; (3) Test 3: the constant current charge/discharge tests of the pouch cell to measure the overpotential resistance by the *V–I* characteristics method and the energy method; (4) Test 4: the direct measurement of heat generation rate with the ARC. The detailed experimental design and parameter settings of these four tests are presented below.

Measurement of the entropy coefficient

An environment chamber GDJW-225 (Yashilin, China) and a six and half voltage monitor 34972A (Agilent, USA) were used in this test. The voltage in the equilibrium state

Table 1 The specifications of the two cells

Cell specification	Value	
	25 Ah cell	Pouch cell
Capacity of 1/3 C at 25 °C	25 Ah	288 mAh
Size	16 × 20 cm^2	8 × 10 cm^2
Number of active electrode pairs	33	2
Cathode material	$LiMn_xCo_yNi_zO_2$ and $LiMn_2O_4$	
Anode material	Graphite	
Nominal voltage	3.8 V	
Recommended charging method	CC-CV	
EODV/end of discharge voltage	3 V	
EOCV/end of charge voltage	4.2 V	

was recorded at four temperatures (5, 15, 25, 35 °C) as well as eleven SOCs (from 1.0 to 0, in a step length of 0.1), and a threshold value of voltage changing rate (voltage changing in a rate less than 0.1 mV/30 min) was preset to control the timing of equilibrium potential measurement.

Intermittent charge/discharge tests of the 25 Ah cell

Only pulse charge and discharge were conducted on the 25 Ah cell since continuous charge or discharge would lead to both significant temperature rise and variation, making it difficult to define a representative temperature for the estimated irreversible heat generation rate. During the intermittent charge/discharge tests, the 25 Ah cell regulated to a definite SOC was charged at 0.1 C for 2 min (except at SOC = 1.0 where the 25 Ah cell was discharged first) and then discharged with the same current back to the original state after 8 min of rest. The above experiment was repeated at 11 SOCs (from 1.0 to 0, step = 0.1), four temperatures (5, 15, 25, 35 °C) and five charging/discharging C-rates (0.1, 0.3, 0.5, 0.7, 0.9 C).

Constant current charge/discharge tests of the pouch cell

The constant current charge/discharge tests of the pouch cell at 0.3, 0.5, 0.7, 0.9, 1.1, 1.3, 1.5 C were performed at cell temperatures of 5, 15, 25, and 35 °C, respectively. In order to verify the effectiveness of the pouch cell to suppress the temperature rise during battery cycling, one thermocouple was attached on the surface of the cell.

Direct measurement of the heat generation rate with the ARC

The basics about how the ARC works was introduced elsewhere [23]. Li et al. [6] observed significant spatial temperature variations in a 25-Ah cell of the same type using thermocouples embedded at 12 locations inside the cell and another 12 thermocouples attached at the corresponding locations on the surface. After analyzing the temperature data of these 12 locations inside and outside battery in [6], we selected two locations that closely represented the cell average temperature during charge/discharge to place the feedback thermocouples on the surface of the 25-Ah cell. Another 12 thermocouples were attached on the surface of the 25 Ah cell as shown in Fig. 1. The cell was connected to a battery cycler made by Arbin (USA) and was charged and then discharged at 1C. The initial temperature of the environment chamber was set as 30 °C. The threshold temperature rising rate in the feedback-and-chasing mode of the ARC was set as 0.02 K min^{-1}.

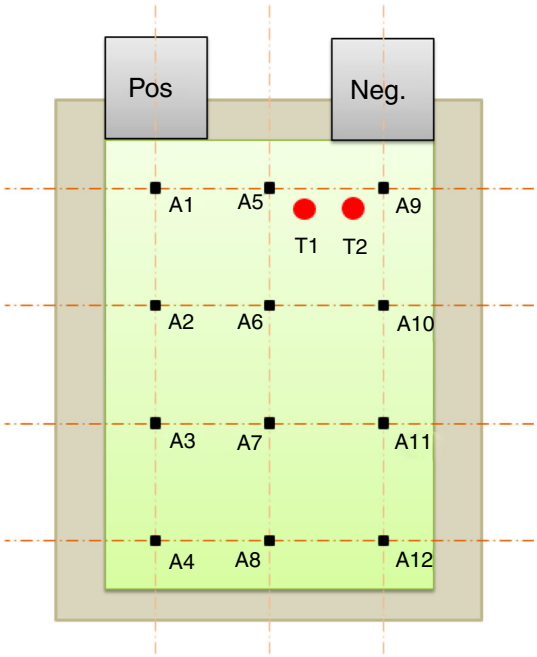

Fig. 1 A schematic plot of the locations of thermocouples

Results and discussion

The entropy coefficient (dU/dt)

The equilibrium potential of the 25 Ah cell was found to be almost linear with respect to the temperature, and the slope of this fitted "potential-temperature" line gave the entropy coefficient, dU/dt. It should be noted that when the SOC was above 0.8 and the ambient temperature was above 25 °C, the self-discharge of the cell was significant. Therefore, under this circumstance, only the equilibrium potentials at lower temperatures were used in the linear fitting to diminish the influence of self-discharge. The entropy coefficient is plotted in Fig. 2 as a function of SOC. The results of the three cells showed good consistency, therefore, only the result of one cell is shown here for concise.

In Fig. 2, the entropy coefficient is negative and shows a sharp increase for SOC < 0.2. When the SOC increases from 0.3 to 0.5, the entropy coefficient turns to be positive and reaches its peak value at SOC = 0.5. After this peak, the entropy coefficient tends to decrease till SOC = 0.7. The minimum value of the entropy coefficient around SOC = 0

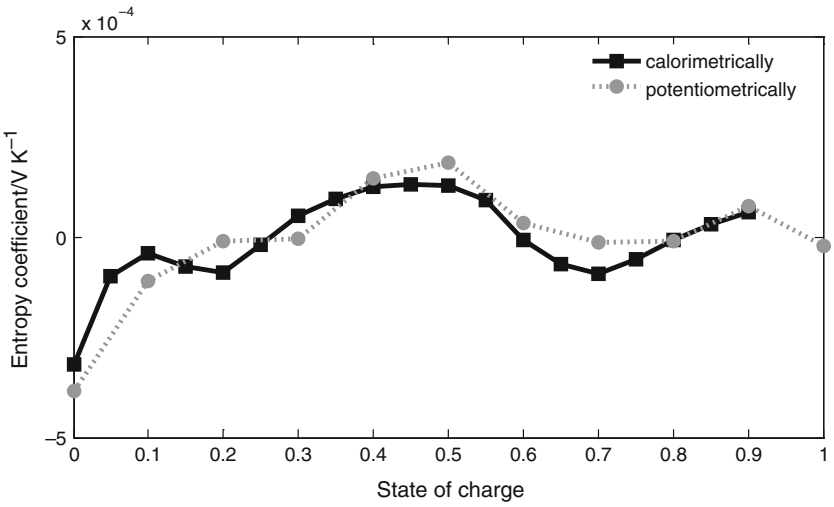

Fig. 2 The entropy coefficient at different SOCs by the calorimetric method and the potentiometric method

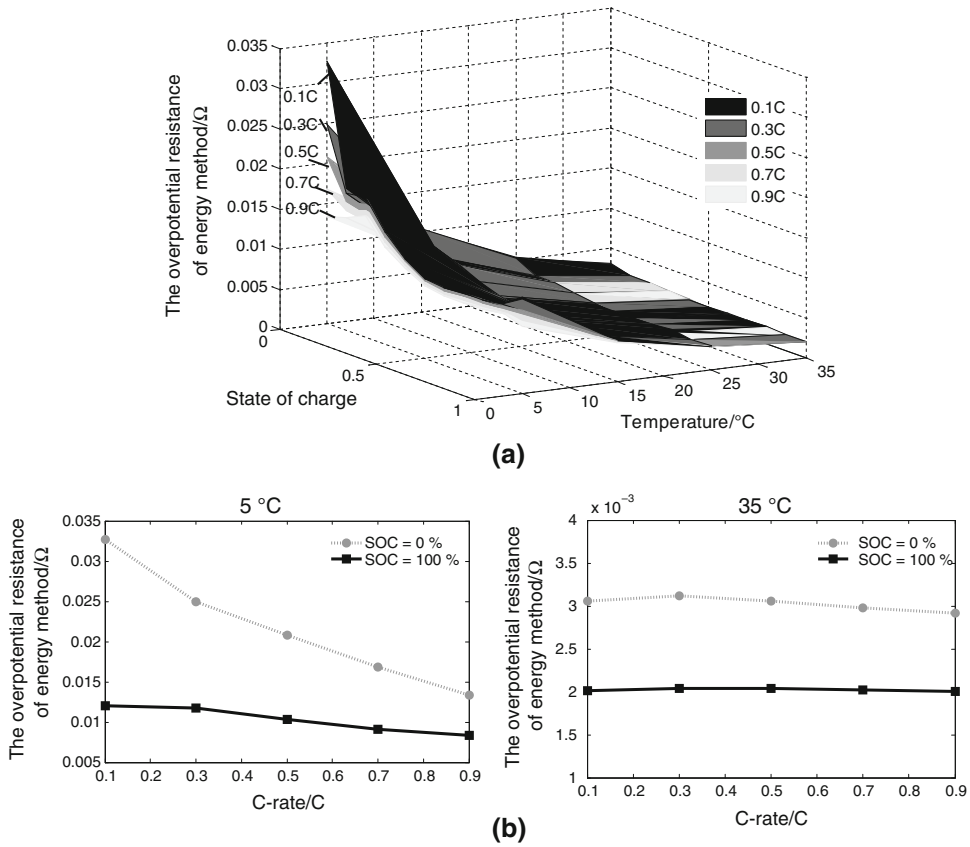

Fig. 3 **a** The overpotential resistance of the 25 Ah cell by the energy method, R_{EM}, as a function of temperature, SOC and C-rate. **b** The effect of the C-rate on the overpotential resistance of the 25 Ah cell by the energy method

is ascribed to the graphite anode (refer to Fig. 4 in [23]). Meanwhile, both the peak at SOC = 0.5 and the valley at SOC = 0.7 are possibly related to the cathode material of $LiMn_2O_4$ (refer to Fig. 1 in [25]). The features shown in Fig. 2 are similar to those in literatures (refer to Fig. 7 in [24] and Fig. 1 in [25]). However, since the composition of electrode materials in this study is not identical with that in the literatures, no further attempt is made to compare these results quantitatively.

Measurement of the overpotential resistance

The overpotential resistance of the 25 Ah cell by the energy method

According to Eq. (12), the overpotential resistance of the 25 Ah cell by the energy method was calculated from the data of the intermittent charge/discharge tests. As shown in Fig. 3a, the R_{EM} is a nonlinear function of temperature,

SOC and C-rate. In addition, as shown in Fig. 3b, the R_{EM} follows a negative correlation with the C-rate. Similar phenomenon has also been observed by Lu and Prakash [17]. There are several possible reasons. First, the charge transfer resistance is smaller at higher C-rates according to Butler–Volmer equation [26]. Second, even though the ambient temperature is controlled by the thermostat, more heat is actually generated inside the cell during charge/discharge at higher C-rates. This results in a transient higher internal temperature of the cell and leads to a decrease of the R_{EM}. Furthermore, it indicates that the C-rate dependency of the R_{EM} is more significant at lower temperatures and smaller SOCs, because the C-rate dependency is weakened when the SOC approaches 1.0, and is negligible when the temperature is 35 °C.

It should be noted that the energy method is based on the assumption that the irreversible heat generation rate during charge is the same as that during discharge. Therefore, the R_{EM} of charge and discharge are not distinguished in this section.

The overpotential resistance of the 25 Ah cell by the intermittent current method

The overpotential resistance of the 25 Ah cell by the intermittent current method, R_{IC}, was calculated by applying the Eq. (12) to the data of intermittent charge/discharge tests with a specific t, which equals 60 s in Fig. 4. Figure 4 shows that the R_{IC} decreases with the increase of temperature, SOC or C-rate, which is quite similar with that of the R_{EM} in "The overpotential resistance of the pouch cell by the *V–I* characteristics method" section. However, unlike that of R_{EM}, the R_{IC} during charge and discharge can be calculated, respectively. It is shown in Fig. 4c that the R_{IC} during discharge is larger than that during charge at lower SOC ranges, while the R_{IC} during charge is larger at some higher SOCs. This phenomenon is confirmed by other methods in this study ("The overpotential resistance of the pouch cell by the *V–I* characteristics method" section) and the mechanism is to be explained later in "The overpotential resistance of the pouch cell by the *V–I* characteristics method" section.

The overpotential resistance of the pouch cell by the V–I characteristics method

A thermocouple was attached to the surface of the pouch cell to verify the effectiveness of using the pouch cell to avoid the significant temperature rise. Due to the small capacity and large heat dissipation surface of the pouch cell, the temperature rise during charge and discharge at 1C was found to be less than 1 °C.

A linear relationship between the terminal voltage and the constant current is detected at most SOCs except when SOC equals 0.0 during charge and 0.1 during discharge. The slope of the *V–I* curve gave the overpotential resistance of charge and discharge by the *V–I* characteristics method, R_{VI}. Figure 5 indicates that the R_{VI} of discharge is larger than that of charge when the SOC is smaller than 0.4. When the SOC increases further, the R_{VI} of charge exceeds

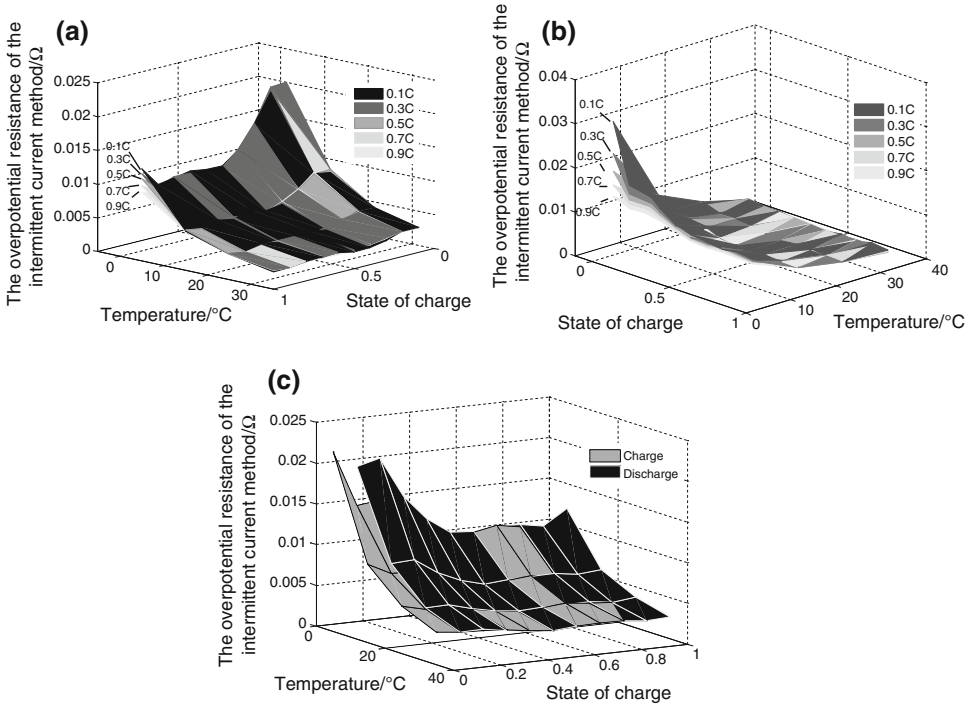

Fig. 4 The overpotential resistance of the 25 Ah cell by the intermittent current method, R_{IC}, as a function of temperature and SOC (t equals 60 s). **a** Charge, **b** discharge, **c** a comparison between charge and discharge at various SOCs and temperatures (the current effect is averaged)

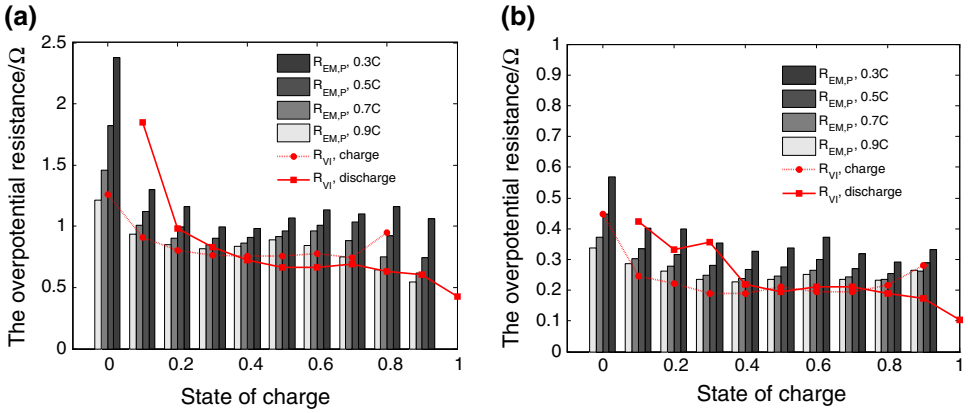

Fig. 5 The overpotential resistances of the pouch cell by the *V–I* characteristics method and energy method as a function of SOC at various temperatures. **a** 5 °C, **b** 35 °C

that of discharge. The underlying reasons were studied in [27] using both the current-interrupt technique in the time-domain and the dynamic electrochemical impedance spectroscopy (DEIS) in the frequency-domain. It was found that the charge transfer resistance and the diffusion resistance during charge are larger than those during discharge under high SOCs, while the situation is opposite at low SOCs. Furthermore, using a half-cell, the charge transfer resistances during charge and discharge of one electrode were compared using the DEIS [28]. It was contended that due to the dependency of the exchange current on the surface concentration and due to the surface concentration variation during intermittent charge/discharge, the charge transfer resistances, which are related to the exchange current, are different between charge and discharge, and specifically, that of discharge is usually larger than that of charge [28].

The overpotential resistance of the pouch cell by the energy method

When the pouch cell is charged or discharged at constant currents, Eq. (11) could be written as:

$$R_{\mathrm{EM}} = \frac{V_{\mathrm{cha}} - V_{\mathrm{dis}}}{2I} \tag{14}$$

where V_{cha} and V_{dis} are the terminal voltage of the pouch cell under charging and discharging with the current I at a specified SOC. Equation (14) was applied to process the data of the constant-current charge/discharge tests, and the calculated overpotential resistance of the pouch cell by the energy method, denoted as $R_{\mathrm{EM,P}}$ or "R_{EM} of pouch cell", is shown in Fig. 5 as a function of SOC and temperature.

Figure 5 shows that the $R_{\mathrm{EM,P}}$ is inversely correlated with the charge/discharge C-rate, which is similar to the R_{EM} in "The overpotential resistance of the 25 Ah cell by the energy method" section, and generally larger than the R_{VI}. Two considerations are presented as follows. First, the explanation concerning why the R_{EM} is inversely correlated

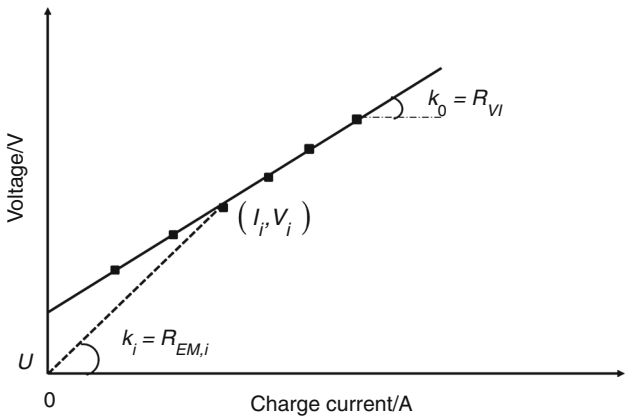

Fig. 6 A schematic plot of the explanation why the $R_{\mathrm{EM,P}}$ holds an inverse proportion to the charge/discharge C-rate and is generally larger than the R_{VI}

with the C-rate is also feasible in the case of the $R_{\mathrm{EM,P}}$. Second, a possible explanation for the relationship between the value of the $R_{\mathrm{EM,P}}$ and that of the R_{VI} is shown in Fig. 6. In the *V–I* characteristics method, when extending the *V–I* line to zero-current, the zero-current voltage is possibly larger (smaller) than the equilibrium potential U during charge (discharge). Therefore, the slope of the solid *V–I* line in Fig. 6, which gives the R_{VI}, is smaller than the slope of the dotted line connecting the two points (I_{i}, V_{i}) and (0, U), which corresponds to the $R_{\mathrm{EM,P}}$. In addition, when the applied current I_{i} is larger, the slope of the dotted line becomes smaller. Therefore, it is another approach to show that the $R_{\mathrm{EM,P}}$ tends to decrease when the applied current C-rate is increased.

Measurement of the heat generation rate of the 25 Ah cell with the ARC

Figure 7 shows the average temperature rising rates of the 25 Ah cell during charge and discharge at 1C in an adiabatic environment provided by the ARC. Since there exists a response delay of the surface temperature rise to the internal

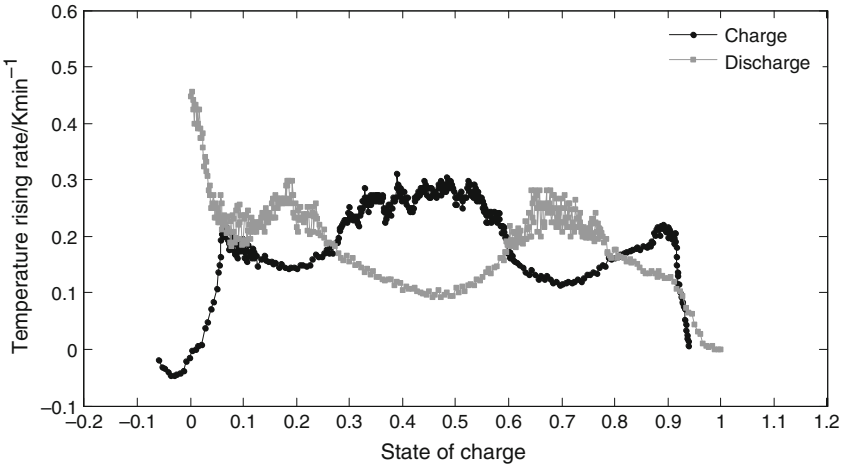

Fig. 7 The average temperature rising rate of the 25 Ah cell during charge/discharge at 1C in the ARC

heat generation and the discharge and charge processes proceed along opposite SOC directions, a peak of internal heat generation rate at a specific SOC could stimulate a delayed temperature rising rate peak at a smaller SOC during discharge and a larger SOC during charge. Therefore, the time delay was compensated by shifting the curve of charge to the left with $\Delta SOC = 0.08$ in Fig. 7, which shows that the heat generation rates of charge and discharge are almost symmetrical as expected [18].

As shown in Fig. 7, at the very beginning of charge, the temperature rising rate is negative. It turns positive and increases sharply, leading to the first exothermic peak around SOC = 0.1. When the SOC further increases to 0.2, a shallow valley of the temperature rising rate is observed. Then a large exothermic plateau shows up in the SOC range of 0.3–0.6. At SOC > 0.7, the temperature rising rate increases again, and then decreases sharply after SOC = 0.9 due to the decreasing charge current during the CV stage in the charge pattern. The temperature rising rate for the discharge exhibits an essentially symmetric profile to that for the charge.

Based on the measured heat generation rate in the ARC, the entropy coefficient was calculated from Eq. (7) and the result was compared with that from the potentiometric method in "The entropy coefficient (dU/dt)" section. As shown in Fig. 2, a good qualitative agreement is found between these two results. However, at SOC < 0.2 and SOC > 0.6, the difference between the dU/dT obtained by the potentiometric method and that by the calorimetric method is more significant than other SOCs. The causes are analyzed as follow.

As shown in Fig. 5, the difference between the overpotential resistance during charge and discharge was also more remarkable at SOC < 0.2 and SOC > 0.6. This means that at these SOCs, the irreversible heat generation rates are not identical during charge and discharge. Therefore, the fundamental assumption in the calorimetric method becomes questionable and the accuracy of the calorimetric method to calculate the entropy coefficient could hardly be satisfactory.

Despite its relatively low accuracy, the calorimetric method is more time efficient to estimate the entropy coefficient. The potentiometric method took almost 1 month to get the entropy coefficient point by point in this study. Relatively, the calorimetric method only cost a few hours to obtain the entropy coefficient of the total SOC range at a time.

Validation of the calculated cell temperature rising rate and the cell temperature

The rising rate of the average cell temperature of the 25 Ah cell in an adiabatic environment can be calculated according to Eq. (15), which is obtained after combining Eq. (2–4) and Eq. (13):

$$\frac{dT}{dt} = \frac{1}{mC_p}\left[I^2R + IT \cdot \left(\frac{\partial U}{\partial T}\right)_P\right]. \tag{15}$$

The major terms in Eq. (15) and their determination methods are summarized in Table 2. In addition, the following three issues need to be addressed to enable the calculation as well as a meaningful validation:

(1) The conversion of the overpotential resistance from the pouch cell to the 25 Ah cell. The area specific overpotential resistance of the pouch cell and that of the 25 Ah cell are expected to be equivalent. Therefore, the overpotential resistance of the 25 Ah cell was converted from that of the pouch cell according to the following equation:

$$R_{25Ah} \cdot A_{25Ah} = R_s \cdot A_s \tag{16}$$

where R_s is the overpotential resistance of the pouch cell and $R_{25\ Ah}$ is the corresponding overpotential resistance of the 25 Ah cell. A_s and $A_{25\ Ah}$ are the

Table 2 The terms in Eq. (15) and their determination methods

Terms	Meaning	Determination method		Source or corresponding section
Cp/ J g^{-1} K^{-1}	The thermal capacity	Calculating from the applied heat and temperature rise in ARC		[29]
m/g	Mass	Weighing		None
$\left(\frac{\partial U}{\partial T}\right)_p$/V K^{-1}	The entropy coefficient	The potentiometric method		See "The entropy coefficient (dU/dt)" section
R/Ω	The overpotential resistance	25 Ah cell	The energy method	See "The overpotential resistance of the 25 Ah cell by the energy method" section
			The intermittent current method	See " The overpotential resistance of the 25 Ah cell by the intermittent current method" section
		Pouch cell	The V–I characteristics method	See "The overpotential resistance of the pouch cell by the V–I characteristics method" section
			The energy method	See "The overpotential resistance of the pouch cell by the energy method" section

active electrode area of the pouch cell and 25 Ah cell, respectively.

(2) The interpolation of the overpotential resistance and the entropy coefficient. The overpotential resistance and the entropy coefficient are estimated at a number of discrete temperature and SOC points. To calculate the overpotential resistance at other SOCs and temperatures during charge/discharge, a 2D look-up table was created and a linear interpolation was utilized in Matlab/Simulink. Similarly, the dU/dT over the full range of SOC was linearly interpolated from the available values at discrete SOCs.

(3) The compensation of the time delay. As stated above, a time delay exists between the rise of the surface temperature and the internal heat generation. Such time delay needs to be compensated to achieve a reliable comparison between the calculated and the measured temperature rising rate of the 25 Ah cell. In this study, a first-order inertial system, as introduced in [6], was assumed as follows:

$$\frac{T_{\text{surf}}(s)}{T_{\text{cal}}(s)} = \frac{1}{1+\tau s} \tag{17}$$

here T_{cal} is the calculated temperature using Eq. (15), and T_{surf} is the corresponding surface temperature. The time constant τ was set as 250 s, which is based on our previous study of the spatial and temporal temperature variation using the same type of the 25 Ah cell [6].

Figure 8 compares the temperature rising rates calculated from Eq. (15) with that measured in ARC of the 25 Ah cell during discharge at 1C. The plot (a) shows the comparison results before the compensation for the time delay, and plot (b) shows the results after the compensation. It is found that a better agreement was achieved after the compensation, especially at the beginning of discharge. The temperature rising rates during charge are compared in Fig. 9. It should be noted that the same reversible heat generation rate was used in calculating each curve in Figs. 8 and 9, while for the irreversible heat generation rate, different overpotential resistances, as shown in Table 2, were used.

The calculated and measured cell temperature curves are displayed in Fig. 10. It should be mentioned that the measured cell temperature was actually the average of 12 thermocouples on the cell surface. As shown in Fig. 10, the slope of temperature curve is relatively steep both at the beginning and the end of discharge, while it is relatively moderate across the middle stage of discharge. In contrast, relatively steep temperature rise occurs in the middle stage of charge at SOC around 0.6. In addition, the average cell temperature increases by 12 °C after discharge at 1C, while it increases by 10 °C, 2 °C smaller, after charge at the same C-rate.

These phenomena can be explained by the following two considerations. First, the reversible heat generation rates during charge and discharge share the identical absolute value but have opposite signs. Therefore, the total reversible heat generation was endothermic during charge and exothermic during discharge, which contributed to a higher cell temperature rise occurred during discharge. Second, with regard to the different temperature rise profiles during charge and discharge, the opposite signs of the reversible heat generation rates accounted for the major differences. In addition, the time delay also made a contribution, for instance, a peak of internal heat generation rate at a specific SOC could stimulate a delayed temperature response at a smaller SOC during discharge and a larger SOC during charge.

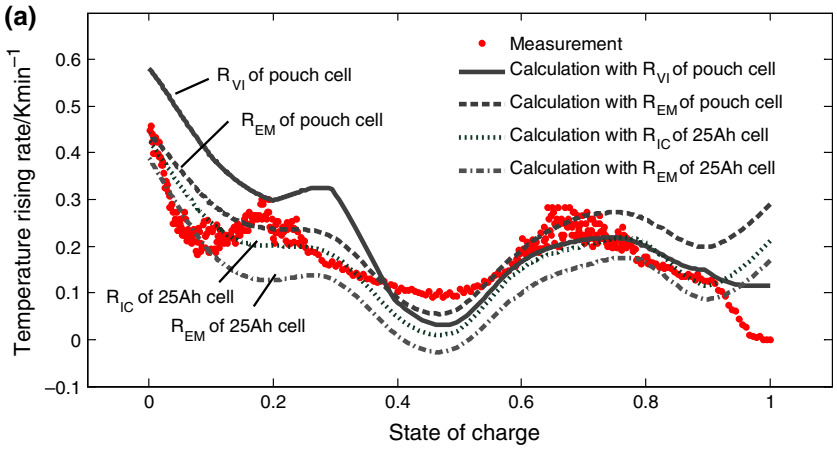

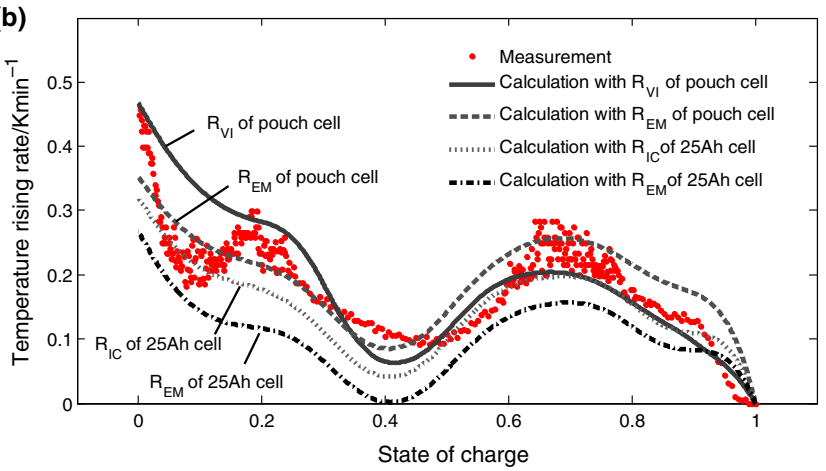

Fig. 8 A comparison between the calculated and experimental temperature rising rate of the 25 Ah cell during discharge at 1 C. **a** Before correction of time delay, **b** after correction of time delay

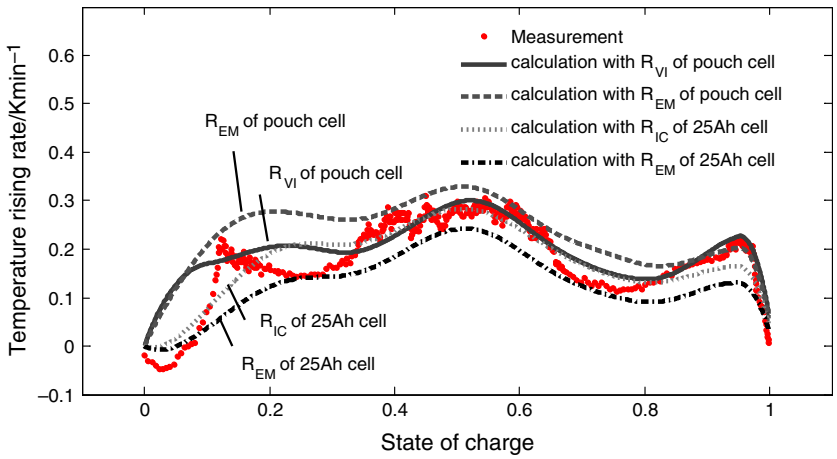

Fig. 9 A comparison between the calculated and experimental temperature rising rate of the 25 Ah cell during charge at 1C

In order to quantitatively compare the four methods estimating the overpotential resistance, the average sum-square error (ASSE) of each method was defined as follows:

$$\mathrm{ASSE} = \frac{1}{N}\sum_{k=1}^{N}\left(\hat{V}_k - V_k\right)^2 \tag{18}$$

where $\hat{V}_k$ is the simulated value (cell temperature or its rising rate), V_k is the corresponding measured value, N is the number of data points.

The ASSE values of the four methods are shown in Table 3. The intermittent current method using the 25 Ah cell yielded the best agreement for the cell temperature rising rate,

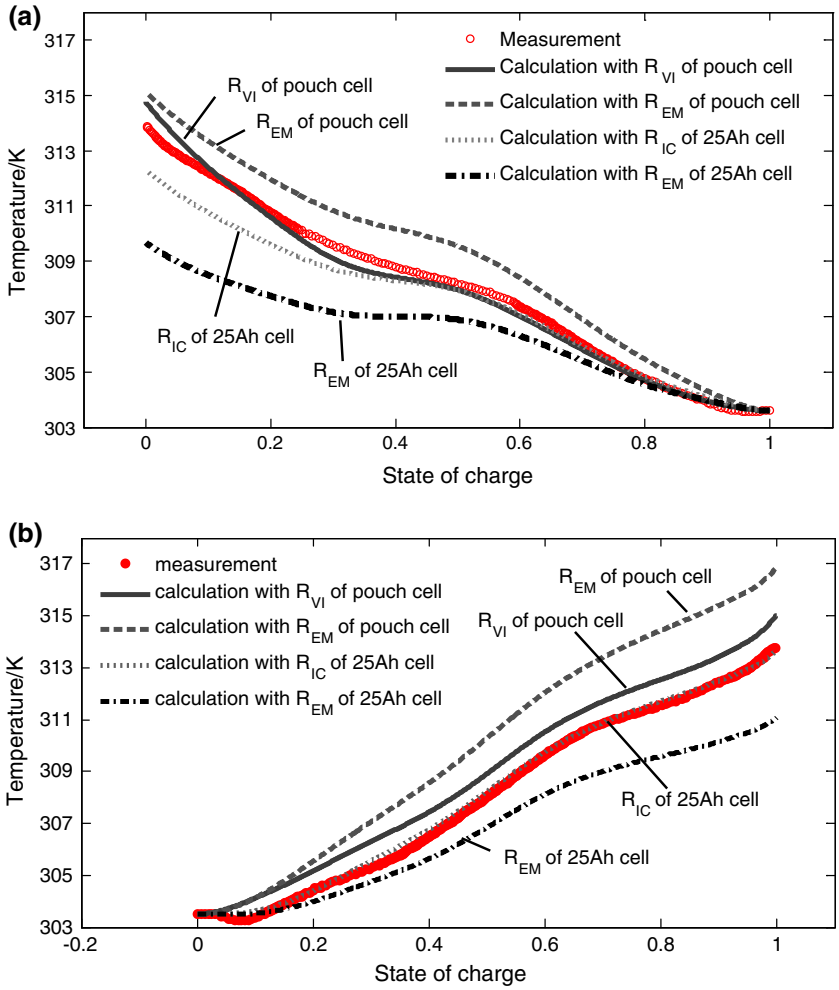

Fig. 10 A comparison between the calculated and experimental cell temperature of the 25 Ah cell during charge and discharge at 1 C. **a** Discharge, **b** charge

followed by *V–I* characteristics method using the pouch cell, and then the energy methods using the 25 Ah cell. With respect to the cell temperature, the best agreement was obtained with the *V–I* characteristics method using the pouch cell, followed by the intermittent current method using the 25 Ah cell. Part of the inaccuracies comes from the influence of reversible heat generation on the overpotential resistance when operating the cells. Further discussion is to be made in the following section.

Discussion of the methods to estimate the irreversible heat

The energy method

As shown in Figs. 8 and 9, the energy method of the 25 Ah cell underestimated the irreversible heat generation rate for both charge and discharge, while the energy method of the pouch cell gave a better agreement. The differences exist in the fact that R_{EM} of the 25 Ah cell comes from the 120 s intermittent charge/discharge test, while the R_{EM} of the pouch cell results from the continuous charge/discharge test. These two tests differ in the test duration, which affects the corresponding R_{EM}. To elucidate the effect of test duration on the energy method and to analyze the under-estimation of R_{EM} of the 25 Ah cell, we take the intermittent charge/discharge test for further analysis. Equation (19) could be deduced from Eq. (12):

$$R_{\mathrm{EM}} = \frac{\sum_{t=0}^{t_d} (V_{\mathrm{cha}} - V_{\mathrm{discha}})}{2IN_{\mathrm{V}}} \tag{19}$$

where t_{d} is the test duration and is 120 s in the intermittent charge/discharge test, N_{V} is the number of the voltage sampling points during the 2 min pulse intermittent charge/discharge, which equals 120 in our tests. Equation (19) indicates clearly that the R_{EM} depends on the test duration, furthermore, it would be greater when the test duration is longer. Since $V_{\mathrm{cha}} - V_{\mathrm{discha}}$ is a convex function with respect to time, Eq. (20) holds:

$$R_{\mathrm{EM}} < \frac{(V_{\mathrm{cha}} - V_{\mathrm{discha}})|_{t=N_{\mathrm{V}}/2}}{2I} = \frac{1}{2}\left(R_{\mathrm{IC,cha}} + R_{\mathrm{IC,dis}}\right). \tag{20}$$

Table 3 Comparison of three methods to estimate the irreversible heat generation rate for large-format lithium-ion batteries

Item		Capable of distinguishing charge and discharge	Dependent on current	ASSE of temperature rising rate prediction		ASSE of cell temperature prediction		Remark
				Dis.	Cha.	Dis.	Cha.	
V–I characteristic method		Yes	No	0.0027	0.0026	0.1035	0.8085	The *V–I* characteristic method should be applied in conjunction with a pouch cell to avoid significant temperature rise. Fabricating a pouch cell with the similar composition may not be convenient in practice.
Energy method	Pouch cell	No	Yes	0.0018	0.0053	1.116	5.0708	The energy method does not require separate set of tests to be conducted. It is versatile in that it can be used to process the data of the *V–I* characteristic method and intermittent current method, as well as the results of other tests. However, it cannot distinguish differences between charge and discharge and is the least accurate one in the three methods.
	25 Ah cell			0.0070	0.0027	4.3751	2.4657	
Intermittent current method		Yes	Yes	0.0011	0.0021	0.5864	0.0284	The intermittent current method is very convenient to use and gives good accuracy if the characteristic time is reasonable selected.

This equation shows that the overpotential resistance calculated by the energy method is smaller than the averaged overpotential resistance of charge and discharge calculated with the intermittent current method in this study. This explains why the energy method yields under-estimation. However, it is noted that Eq. (20) does not always hold when $t < N_v/2$.

In addition, the overpotential resistance results imply that the irreversible heat generation rates are not identical during charge and discharge. In this case, the most important assumption in the energy method becomes questionable and the accuracy of the energy method to calculate the heat generation could hardly be satisfactory. Despite all this, the energy method is still a valuable method in that it does not require extra tests, instead, it can be directly applied to the test data of the *V–I* characteristic method and the intermittent current method.

The intermittent current method

A good agreement was obtained when the intermittent current method with an interval of 60 s was used to estimate the irreversible heat generation rate. However, the accuracy of the intermittent current method depends strongly on the interval. Figure 11 plots the calculated cell temperature rising rate at various intervals and the corresponding ASSEs. It is clear that the ASSE decreases sharply when the interval increases from 10 to 60 s. Afterwards, the ASSE exhibits a relatively flat trend and its minimum value is achieved at the interval of 90 s.

The irreversible heat is composed of the heat generated by the activation (interfacial kinetics), the concentration (diffusion process), and the ohmic losses. The ohmic loss is essentially instantaneous, and the characteristic frequency associated with the interfacial reaction is normally much higher than 1 Hz in ambient temperature. The characteristic time of the diffusion process is expressed as:

$$t_d \approx L^2/D \tag{21}$$

where L is the characteristic length of the diffusion process and D is the diffusion coefficient. From Eq. (21), it is clear that t_d differs for different battery systems and is affected by temperature due to the strong temperature dependency of the diffusion coefficient. Order of magnitude analysis shows that the t_d is about 10^2–10^3 s in this study.

As the interval used in this study is much larger than 1 s, but smaller than the t_d, we believe that the estimated rate of irreversible heat generation is attributed to the ohmic loss, the charge transfer loss, and part of the diffusion loss. A different interval determines a different percentage of the total diffusion loss included in the calculation, which could result in a different overpotential resistance and affect the

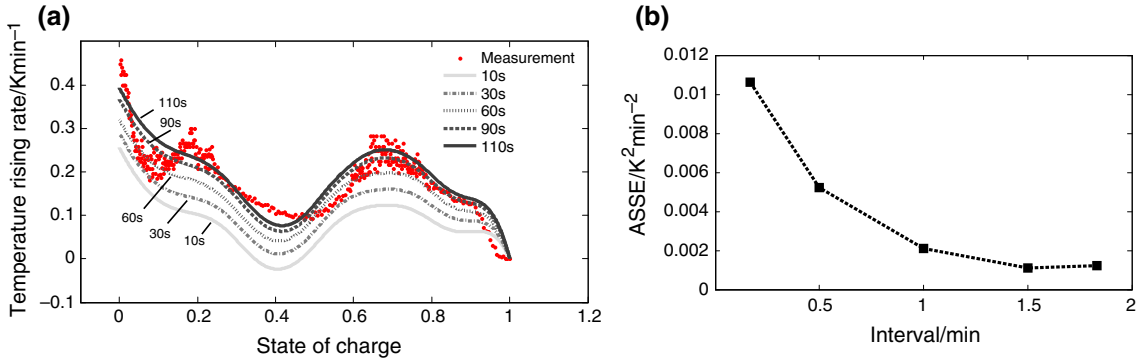

Fig. 11 **a** The effect of the interval on the cell temperature rising rate calculated through the overpotential resistance of the 25 Ah cell by the intermittent current method. **b** The average sum-square error at various intervals

prediction accuracy. However, as can be seen from Fig. 11, when the interval is between an appropriate range, which is between 60 and 120 s in this study, the influence of interval on the ASSE is negligible. Therefore, it is essential to examine the ASSE at multiple intervals; afterwards, an appropriate one can be selected.

The V–I characteristic method

The *V–I* characteristic method was applied to a pouch cell instead of the 25 Ah large-format cell to avoid the significant temperature rise during continuous charge/discharge of large cells. From Table 3, it is found that the *V–I* characteristic method using the pouch cells is an effective method to estimate the irreversible heat generated by the large-format cells. However, due to the necessity of fabricating pouch cells, this method is not as convenient as other methods in practice.

With respect to the *V–I* characteristic method, an overestimation of heat generation rates at low SOC range between 0 and 0.2 was detected, especially during discharge, as shown in Figs. 8 and 9. The underlying reason can be ascribed to the nonlinear current dependency of terminal voltage at low SOC ranges. To be specific, the nonlinear current dependency of terminal voltage at SOC = 0.1 during discharge magnified the overpotential resistance, and then the estimated heat generation rate was enlarged.

The features of these three methods, i.e., the *V–I* characteristic method (using the pouch cell), the energy method (using both the pouch cell and 25 Ah cell), the intermittent current method (using the 25 Ah cell) are summarized in Table 3.

Conclusions

The heat generation rate of a large-format 25-Ah lithium-ion battery was studied based on the simplified Bernardi heat generation model. The heat generation rate was divided into the reversible and irreversible heat terms, with each term being estimated with different methods and subsequently validated against measured temperature rise.

The methods developed for small lithium-ion batteries were extended to the large-format 25 Ah lithium-ion battery with the following techniques employed:

(1) A pouch cell, using the same electrodes as the 25 Ah cell but with a simple structure as well as a much smaller capacity, was employed in the *V–I* characteristics method to avoid the significant temperature rise of large cells during charge and discharge. The overpotential resistance of the pouch cell was converted to that of the 25 Ah cell based on the concept of equivalent area-specific resistances.
(2) Twelve thermocouples were used for calculating the average cell temperature to accommodate the temperature variations across the cell.
(3) The first-order inertial system was assumed to correct the delay in the response of the surface temperature to the internal heat generation, and the time constant of the system was set as 250 s in this study.

Then, the accuracy of different methods was compared and the main features of these methods were elucidated and summarized as follows:

(1) In calculating the reversible heat, the entropy coefficient measured with the potentiometric method was believed to be more accurate, while the calorimetric method was more efficient. The less accuracy of the latter method partly comes from its assumption that the irreversible heat generation rates of charge and discharge are identical.
(2) The irreversible heat was estimated by calculating the overpotential resistance of the cell. Among the three methods to measure the overpotential resistance, the intermittent current method is both easy-to-implement and accurate if the interval is appropriately

chosen. For the 25 Ah cell in this study, it is found that the error of the intermittent current method remained small when the interval was in the range of 60 to 120 s. With the help of a pouch cell, the *V–I* characteristic method was proven to achieve comparable accuracy. However, the necessity of fabricating a pouch cell incurs some inconvenience for this method. The newly developed energy method does not require extra tests, instead, it can be directly applied to the test data of the *V–I* characteristic method and the intermittent current method. However, it cannot distinguish between charge and discharge and it is the least accurate among these three methods.

Acknowledgements This study was supported by the National Natural Science Foundation of China under the grant number of 51207080, the Independent Research Programs of Tsinghua University under the subject number of 2011Z01004, and the China Postdoctoral Science Foundation under the Grant number of 2012M510436.

References

1. Yang K, An JJ, Chen S. Temperature characterization analysis of $LiFePO_4$/C power battery during charging and discharging. J Therm Anal Calorim. 2010;99:515–21.
2. Jhu CY, Wang YW, Wen CY, Chiang CC, Shu CM. Self-reactive rating of thermal runaway hazards on 18650 lithium-ion batteries. J Therm Anal Calorim. 2011;106:159–63.
3. Jhu CY, Wang YW, Wen CY, Chiang CC, Shu CM. Thermal runaway features of 18650 lithium-ion batteries for $LiFePO_4$ cathode material by DSC and VSP2. J Therm Anal Calorim. 2011;106:159–63.
4. Lu TY, Chiang CC, Wu SH, Chen KC, Lin SJ, Wen CY, Shu CM. Thermal hazard evaluations of 18650 lithium-ion batteries by an adiabatic calorimeter. J Therm Anal Calorim. 2013. doi:10.1007/s10973-013-3137-9.
5. Yang K, Li DH, Chen S, Wu F. Thermal behavior of nickel/metal hydride battery during charging and discharging. J Therm Anal Calorim. 2009;95:455–9.
6. Li Z, Zhang J, Wu B, Huang J, et al. Examining temporal and spatial variations of internal temperature in large-format laminated battery with embedded thermocouples. J Power Sources. 2013;241:536–53.
7. Yang K, An JJ, Chen S. Influence of additives on the thermal behavior of nickel/metal hydride battery. J Therm Anal Calorim. 2010;102:953–9.
8. Hallaj SA, Maleki H, Hong JS, Selman JR. Thermal modeling and design considerations of lithium-ion batteries. J Power Sources. 1999;83:1–8.
9. Billy W, Vladimir Y, Monica M, Gregory JO, Ricardo FM, Nigel PB. Coupled thermal-electrochemical modelling of uneven heat generation in lithium-ion battery packs. J Power Sources. 2013;243:544–54.
10. Gu WB, Wang CY. Thermal-electrochemical modeling of battery systems. J Electrochem Soc. 2000;147:2910–22.
11. Bernardi D, Pawlikowski E, Newman J. A general energy balance for battery systems. J Electrochem Soc. 1985;132(1):5–12.
12. Onda K, Kameyama H, Hanamoto T, Ito K. Experimental study on heat generation behavior of small lithium-ion secondary batteries. J Electrochem Soc. 2003;150:A285–91.
13. Onda K, Ohshima T, Nakayama M, Fukuda K, Araki T. Thermal behavior of small lithium-ion secondary battery during rapid charge and discharge cycles. J Power Sources. 2006;158:535–42.
14. Ohshima T, Nakayama M, Fukuda K, Araki T, Onda K. Thermal behavior of small lithium-ion battery during rapid charge and discharge cycles. Electr Eng Jpn. 2006;157:1521–8.
15. Hallaj SA, Venkatachalapathy R, Prakash J, Selman JR. Entropy changes due to structural transformation in the graphite anode and phase change of the $LiCoO_2$ cathode. J Electrochem Soc. 2000;147:2432–6.
16. Hallaj SA, Prakash J, Selman JR. Characterization of commercial Li-ion batteries using electrochemical-calorimetric measurements. J Power Sources. 2000;87:186–94.
17. Lu W, Prakash J. In situ measurements of heat generation in a Li/mesocarbon microbead half-cell. J Electrochem Soc. 2003;150:A262–6.
18. Yang H, Prakash J. Determination of the reversible and irreversible heats of a $LiNi_{0.8}Co_{0.15}Al_{0.05}O_2$/natural graphite cell using electrochemical-calorimetric technique. J Electrochem Soc. 2004;151:A1222–9.
19. Bang H, Yang H, Sun YK, Parakash J. In situ studies of $Li_xMn_2O_4$ and $Li_xAl_{0.17}Mn_{1.83}O_{3.97}S_{0.03}$ cathode by IMC. J Electrochem Soc. 2005;151:A421–8.
20. Thomas KE, Bogatu C, Newman J. Measurements of the entropy of the reaction as a function of sate of charge in doped and undoped lithium manganese oxide. J Electrochem Soc. 2001;148:A570–5.
21. FreedomCAR Battery Test Manual for Power-Assist Hybrid Electric Vehicles, DOE/ID-11069, Idaho National Engineering and Environmental Laboratory, Draft, April 2003
22. Lv Z, Guo X, Qiu X. New Li-ion battery evaluation research based on thermal property and heat generation behavior of battery. Chin J Chem Phys. 2012;25:725–32.
23. Ishikawa H, Mendoza O, Sone Y, Umeda M. Study of thermal deterioration of lithium-ion secondary cell using an accelerated rate calorimeter (ARC) and AC impedance method. J Power Sources. 2012;198:236–42.
24. Williford RE, Viswanathan VV, Zhang J. Effects of entropy changes in anodes and cathodes on the thermal behavior of lithium-ion batteries. J Power Sources. 2009;189:101–7.
25. Viswanathan VV, Choi D, Wang D, Xu W, Towne S, Williford RE, Zhang J, Liu J, Yang Z. Effect of entropy change of lithium intercalation in cathodes and anodes on Li-ion battery thermal management. J Power Sources. 2010;195:3720–9.
26. Moss PL, Au G, Plichta EJ, Zheng JP. An electrical circuit for modeling the dynamic response of Li-ion polymer batteries. J Electrochem Soc. 2008;155:A986–94.
27. Zhang J, Huang J, Li Z, Song S, Song W, Wu N. The study of resistance variation between charging and discharging process by current-interrupt technique and dynamic electrochemical impedance spectroscopy (DEIS). 2013 IEEE vehicle power and propulsion conference (VPPC), Beijing, China, 15–18 Oct 2013.
28. Huang J, Li Z, Zhang J, Song S, Wu N. Exploring differences between charging and discharging of $Li_xMn_2O_4$/Li half-cell with dynamic electrochemical impedance spectroscopy (DEIS). The 9th international symposium on electrochemical impedance spectroscopy, Okinawa, Japan, 17–21 June 2013.
29. Zhang J, Wu B, Zhe L, Huang J. Simultaneous estimation of multiple thermal parameters of large-format laminated lithium-ion batteries. 2013 IEEE vehicle power and propulsion conference (VPPC), Beijing, China, 15–18 Oct 2013.